Redox Biology 57 (2022) 102492

Contents lists available at ScienceDirect

Redox Biology

journal homepage: www.elsevier.com/locate/redox

RNA binding protein IGF2BP1 meditates oxidative stress-induced granulosa cell dysfunction by regulating *MDM2* mRNA stability in an m^{6}A-dependent manner

Hongbei Mu [a,1], Siying Cai [a,1], Xiaofei Wang [a], Huiying Li [a], Ling Zhang [a,b,***], Huaibiao Li [a,**], Wenpei Xiang [a,b,*]

[a] Institute of Reproductive Health, Tongji Medical College, Huazhong University of Science and Technology, Wuhan, China
[b] Wuhan Tongji Reproductive Medicine Hospital, 128 Sanyang Road, Wuhan 430013, China

ARTICLE INFO

Keywords:
IGF2BP1
Granulosa cells
Oxidative stress
m^{6}A modification
Cellular senescence
Reactive oxygen species

ABSTRACT

Both genetic and microenvironmental detrimental factors are involved in ovarian dysfunction, leading to the increasing rate of involuntary childlessness in recent years. Oxidative stress (OS), which is characterized by the imbalance of redox system with redundant reactive oxygen species (ROS) overwhelming the antioxidant defense, is regarded as one of the culprits of ovarian dysfunction. OS causes damage to various types of ovarian cells including granulosa cells (GCs), jeopardizing the ovarian microenvironment, disturbing follicular development and participating in various female reproductive disorders. However, the specific molecular pathological mechanisms underlying this process have not been fully elucidated. In this study, we found that 3-nitropropionic acid (3-NP) treatment led to significant IGF2BP1 downregulation via, at least partially, inducing ROS overproduction. IGF2BP1 regulates GCs viability, proliferation, cell cycle and cellular senescence by enhancing *MDM2* mRNA stability in an m^{6}A-dependant manner. IGF2BP1 overexpression partially rescued 3-NP induced GCs damages, while ectopically expressed MDM2 alleviated both 3-NP or IGF2BP1-knockdown induced GCs dysfunction. These results reveal an epigenetic molecular mechanism underlying OS-related GCs disorders, which may help to establish a novel potential clinical marker for predicting the GCs status as well as the follicular developmental potential.

1. Introduction

Postponement of parenthood, unhealthy lifestyle, environmental pollution and mental stress are progressively increasing the rate of involuntary childlessness [1,2]. In recent years, multifactorial female infertility has gradually become one of the most arduous problems of reproductive medicine. However, the mechanisms underlying female infertility have not been fully elucidated yet. Substantial evidences have revealed that both genetic and microenvironmental factors are involved in female fertility decline. These etiologies collectively contribute to the diminished ovarian reserve, ultimately resulting in impaired female fecundity [3].

Among all the infertility-inducing factors, oxidative stress (OS) is regarded as one of the culprits of ovarian dysfunction. As a result of the imbalance of redox system, OS causes damages to cells and tissues with redundant reactive oxygen species (ROS) overwhelming the antioxidant defense. ROS, including peroxides, superoxide, hydroxyl radical and singlet oxygen [4], are highly reactive chemicals derived from the reduction of molecular oxygen. In normal conditions, moderate amount of ROS is generated on the mitochondrial respiratory chain and serves as a signaling molecular enabling several physiological processes [5]. Nevertheless, when ROS accumulate to an extent exceeding the body's

Abbreviations: OS, oxidative stress; GCs, granulosa cells; ROS, reactive oxygen species; 3-NP, 3-nitropropionic acid; FSH, follicle-stimulating hormone; LH, luteinizing hormone; ActD, Actinomycin D; m^{6}A, N6-methyladenosine; UTR, untranslated region.

* Corresponding author. Institute of Reproductive Health, Tongji Medical College, Huazhong University of Science and Technology, Wuhan, China.
** Corresponding author.
*** Corresponding author. Institute of Reproductive Health, Tongji Medical College, Huazhong University of Science and Technology, Wuhan, China.
E-mail addresses: Zhling312@163.com (L. Zhang), lihuaibiao@hust.edu.cn (H. Li), wpxiang2010@hust.edu.cn (W. Xiang).
[1] These authors contributed equally to this work.

https://doi.org/10.1016/j.redox.2022.102492
Received 30 August 2022; Received in revised form 20 September 2022; Accepted 23 September 2022
Available online 24 September 2022

scavenging capacity, it will lead to varying degrees of OS and, in consequence, multiple kinds of cellular damages [6]. OS jeopardizes the ovarian microenvironment, disturbs follicular development and participates in various female reproductive disorders including endometriosis, polycystic ovary syndrome and premature ovarian failure, which make it a key regulator in the pathogenesis of female subfertility [6–8].

Granulosa cells (GCs), a kind of ovarian somatic cell which surrounds and closely correlates with the developing oocytes, are considered as a multifunctional and pivotal component of the ovarian follicular microenvironment. Under the stimulation of follicle-stimulating hormone, the single-layered GCs proliferate into multiple layers and differentiate into two types, the inner cumulus cells which encircle the oocytes and the outer mural GCs which cling to the follicular wall [9,10]. GCs participate in oogenesis by supporting the oocyte development, producing sex steroids and secreting several growth factors [11]. Intact GCs functions are an indispensable prerequisite for acquiring oocyte competence and maintaining female fertility. However, various detrimental factors, including OS, will result in GCs dysfunction and hinder the GCs-oocyte interaction. The adverse impact of OS on GCs has been revealed by several studies. Zhou et al. found advanced oxidation protein products enhanced intracellular ROS generation and caused cell cycle arrest [12]. Another study suggested that excessive OS in cumulus GCs lead to cellular senescence and subsequent endometriosis-associated infertility [13]. Additionally, the function of GCs to produce steroid hormones was also impaired by OS exposure [14]. All these evidences demonstrate that OS will result in GCs dysfunction and impair female fecundity. Despite all that, the specific molecular pathological mechanisms underlying this process have not been fully elucidated.

In this study, we found the treatment of 3-nitropropionic acid (3-NP), a mitochondrial toxin inducing intracellular OS by targeting complex II of electron transport chain, led to significant downregulation of Insulin-like growth factor 2 mRNA-binding protein 1 (IGF2BP1) and subsequently resulted in *MDM2* mRNA instability in GCs. IGF2BP1 is an RNA-binding protein which preferentially binds to m^6A modifications and helps to stabilize its targeted transcripts [15–18]. As a potent oncogenic factor, IGF2BP1 regulates proliferation, cell cycle progression and stemness of cancer cells [17,19,20]. Furthermore, it also modulates cell behaviors in pluripotent and mesenchymal stem cells [21,22]. In recent years, IGF2BP1 was found to be an essential regulator of intestinal functions by facilitating colonic epithelial repair and maintaining the intestinal barrier function [23,24]. All these evidences revealed that IGF2BP1 is involved in various biological processes, especially in cell proliferation. Considering that the massive growth of GCs is a crucial supportive condition for follicular development, we reasoned that IGF2BP1 may also serve as a key factor regulating GCs behavior during folliculogenesis, which has not been, however, evidenced by any study up to now. MDM2 is an essential regulator of p53 in both normal and cancer cells. MDM2 upregulation usually provides proliferation advantages to cells, leading to the progression and metastasis of cancers. MDM2 and p53 modulate each other via an autoregulatory feedback loop, collectively controlling several cellular processes including cell proliferation, cell cycle and cell motility [25–27]. Additionally, MDM2 also participates in several clinically relevant cellular processes in a p53-independent manner [28,29]. Previous studies have revealed the role of MDM2 in regulating GCs apoptosis, proliferation, follicular development and oocyte quality [30–32], indicating MDM2 is a key factor in maintaining normal GCs functions and female fertility. The specific mechanisms by which MDM2 is regulated in GCs, however, still remain unclear.

The present study first revealed the involvement of IGF2BP1 in meditating OS-induced GCs dysfunction. IGF2BP1 downregulation in GCs destabilized *MDM2* mRNA, resulting in impaired cell viability, inhibited cell proliferation, arrested cell cycle and exacerbated cellular senescence. These results decipher a novel OS-related mechanism meditating damages and dysfunctions in GCs, which may facilitate to develop new therapeutic strategies to improve the follicular developmental potential and subsequent reproductive outcomes.

2. Materials and methods

2.1. Animal handling and ethics approvals

Female C57BL/6J mice (8-week-old, SPF-class) were obtained from Charles River, Beijing, China. All mice were adapted for 3 days after their purchase and were maintained under a controlled temperature (26 ± 2 °C) with 12 h (h) light/dark conditions. Fifty mice were randomly dived into two groups (the control group and the 3-NP group, n = 25 per group). Mice in the 3-NP group received intraperitoneal injections of 20 mg/kg 3-NP (diluted with PBS) administration every morning for 2 weeks, while mice in the control group received an equal volume of PBS. The body weight of mice was recorded before and after 3-NP administration. Vaginal smears were obtained before sacrifice to monitor the estrous cycles of mice [33] and subsequent assays were performed using mice at the same phase of estrous cycle. Ovaries were removed and weighed immediately. The ovary coefficient was defined as the ratio of the ovary weight to the body weight of the mouse. For preparation of paraffin sections, the ovaries were immediately fixed in 4% paraformaldehyde, embedded in paraffin, and sectioned into 5-μm-thick slices. For frozen sections, the ovaries were directly immersed in liquid nitrogen, embedded in a freezing compound (OTC) and sectioned into 10-μm-thick slices. The paraffin sections were stained with hematoxylin and eosin (H&E) and imaged using a virtual slide scanner VS120 (Olympus, Japan). All stages of follicles (primordial, primary, small secondary, large secondary and antral follicles) were detected and classified. The number of follicles from each ovary was calculated and compared between each group.

The experiments were approved by the Institutional Animal Care and Use Committee, Huazhong University of Science and Technology in accordance with the National Research Council's "Guideline for the Care and Use of Laboratory Animals".

2.2. Cell culture and treatment

The human granulosa tumor-derived cell line COV434 was purchased from Wuhan Warner Bio Technology Co., Ltd. The human granulosa-like tumor cell line KGN and human embryonic kidney cell line HEK293T were obtained from Procell Life Science&Technology Co., Ltd. All the cells were maintained in Dulbecco's modified Eagle's medium (DMEM, Gibco, USA) supplemented with 10% fetal bovine serum (Gibco, USA) and 1% penicillin/streptomycin (Gibco, USA) at 37 °C in a humidified incubator containing 5% CO_2, and stored in FBS with 10% DMSO at −80 °C. To stimulate ROS production or induce energy depletion, COV434 cells (70% confluence) were treated with 10 mM 3-NP (Sigma-Aldrich, USA), 150 μM hydrogen peroxide (H_2O_2, Sinopharm, China),2.5 μM antimycin A (Maokang biotechnology, China) or 1.5 μM Carbonyl cyanide 4-(trifluoromethoxy)phenylhydrazone (FCCP, MedChemExpress, China) for 24 h. Pretreatment of N-acetylcysteine (NAC, MedChemExpress) was performed at concentration of 2.5 mM for 2h. Transfection of cells with DNA or siRNAs was performed using Lipofectamine 3000 (Thermo Fisher Scientific, USA) according to the manufacturer's instructions. For siRNA-meditated IGF2BP1 or METTL3 knockdown, cells were transfected with 50 nM IGF2BP1- or METTL3-directed siRNA as well as its negative controls (RiboBio, China). For IGF2BP1 or MDM2 overexpression, cells were transfected with pcDNA3.1-IGF2BP1 (Genomeditech Co., Ltd, China) and pCMV-MDM2 (Vigene Biosciences, China) as well as their respective vectors as negative controls. The siRNA sequences used are provided as follows:

si-IGF2BP1: 5′- GGCTCAGTATGGTACAGTA -3'.

si-METTL3: 5′- GCAAGAATTCTGTGACTAT -3'.

2.3. ROS and superoxide anion quantification

A reactive oxygen species assay kit (Beyotime) and superoxide anion indicator (Beyotime) were used following the manufacturers' instructions. The cells were rinsed and incubated with the fluorescent probe DCFH-DA and Dihydroethidium in the dark at 37 °C for 25 min. After 3 washes with DMEM, cells were incubated with Hoechst 33,342 for nuclear staining. Fluorescent images were captured with a Zeiss LSM 900 Confocal Laser Scanning Microscope (Carl Zeiss, Germany). Quantification of ROS or superoxide anion in COV434 cells or ovarian frozen sections was performed by analyzing the fluorescent intensity.

2.4. Cell viability and proliferation assay

Cell viability was determined using the Cell Counting Kit-8 (CCK-8, Yeasen, China). After cell treatment, 10μL/well CCK-8 solution was added to each well of the 96-well plate and incubated at 37 °C for 2 h. The spectrophotometric absorbance increase at 450 nm was measured with a Synergy HTX Multi-Mode Reader (BioTek, USA). Cell proliferation capacity was analyzed with Cell-Light EdU Apollo567 In Vitro Kit (RiboBio, China). Briefly, cells were labeled with EdU by incubating with 50 μM EdU medium for 2 h and were fixed with 4% paraformaldehyde in phosphate buffer saline (PBS). After washed with 2 mg/mL glycine solution for 5 min, cells were permeabilized with 0.5% Triton X-100 in PBS for 10 min and then incubated with 1x Apollo solution for 30min while protected from light. For subsequent DNA staining, cells were incubated with 1x Hoechst 33,342 for 30 min. All the solution used was prepared following the manufacturers' instructions.

2.5. Flow cytometry

The cell cycle phase distribution was determined using the Cell Cycle Analysis Kit (Beyotime, China). Briefly, cells were digested with trypsin and subsequently fixed with 70% ethanol at 4 °C for 12 h. The fixed cells were then stained with PI solution (prepared according to the manufacturers' instructions) at 37 °C for 30 min, and data was acquired using NovoCyte Flow Cytometer Systems (Agilent, USA).

2.6. SA-β-Gal staining

SA-β-Gal staining was performed using a Senescence β-Galactosidase Staining Kit (Beyotime). Cells and frozen sections of mouse ovaries were fixed in fixation solution (provided in the kit) for 15min. Next, cells and frozen sections were incubated with staining solution (prepared according to the manufacturers' instructions) at 37 °C. SA-β-Gal activity was examined after incubation for 48 h.

2.7. Hormone assays

The levels of hormones in the serum were measured using commercialized enzyme-linked immunosorbent assay (ELISA) kits in accordance with the manufacturer's instructions. The ELISA kits for estradiol, progesterone and follicle-stimulating hormone were purchased from Meimian (China). The ELISA kit for luteinizing hormone was from CUSABIO (USA).

2.8. Quantitative real-time PCR (qRT-PCR)

Total RNA was extracted from COV434 cells using RNA-easy Isolation Reagent (Vazyme, China) and reverse-transcribed using HiScript II 1st Strand cDNA Synthesis Kit (Vazyme). For measurement of mRNA targets, qRT-PCR was performed on a Quantagene q225 real-time PCR system (Kubo, China) using Taq Pro Universal SYBR qPCR Master Mix (Vazyme) with custom-designed primers. The RT-qPCR conditions were set as follows: 95 °C for 30 s, followed by 40 cycles of 95 °C for 10 s and 60 °C for 30 s. The relative expression of candidate mRNAs was normalized to β-actin (ACTB) and fold changes were calculated using the $2^{-\Delta\Delta Ct}$ method. All experiments were performed in biological and technical triplicates and presented as the means ± SD. The primer sequences are listed in Supplementary Table 1.

2.9. Western blot

Total protein from the COV434 cells and mouse ovaries was extracted using RIPA reagent (Solarbio, China) supplemented with protease inhibitor cocktails (Abmole, China). After being denatured and separated on a 10% polyacrylamide SDS-PAGE gel, proteins were transferred to a Polyvinylidene fluoride (PVDF) membrane (Millipore, USA). Protein expression was analyzed with indicated primary antibodies by using goat anti-rabbit or anti-mouse HRP-conjugated secondary antibodies. The protein bands were visualized using a electrochemiluminescence (ECL) reagent kit (EpiZyme, China) and imaged with Bio-Rad Gel Imaging Systems (Bio-Rad, USA). Antibodies used are indicated in Supplementary Table 2.

2.10. Immunofluorescence (IF) staining

For cultured cells, COV434 cells were fixed with 4% paraformaldehyde and permeated with 0.5% Triton X-100 in PBS. For mouse ovarian tissue, the paraffin sections were treated with antigen retrieval buffer in boiling after dewaxing and rehydration. The cells and sections were then blocked with goat serum and incubated with indicated primary antibodies and secondary antibodies. For nuclear staining, the cells and sections were incubated with fluorescent dye DAPI staining reagent (Servicebio, China). Fluorescence imaging was performed using a Zeiss Axio Observer 5 fluorescence microscope (Carl Zeiss). Antibodies used are indicated in Supplementary Table 2.

2.11. Measurement of ATP levels

The intracellular ATP levels were measured using an ATP Assay Kit (Beyotime, China). Briefly, COV434 cells were lysed with ATP lysis buffer then the supernatant was collected after centrifugation (12,000 g, 4 °C, 5 min). The working solution was added to the opaque 96-well plate first to deplete background ATP, after which the reference standard and samples were added to the detection well, and the relative light unit (RLU) value was measured with a Synergy HTX Multi-Mode Reader (BioTek). All the solution used was prepared following the manufacturers' instructions.

2.12. RNA-sequencing

Total RNA was isolated from control and 3-NP treated COV434 cells by using Trizol reagent (Invitrogen, USA) as described by the manufacturer. The quality and quantity of RNA samples were assessed with NanoDrop 2000 Spectrophotometer (Thermo Fisher, USA). Library construction and RNA sequencing were performed by Annaroad Gene Technology (Beijing) Co., Ltd. Sequencing reads were aligned to the USCS hg38.0 *Homo sapiens* reference genome using HISAT2 software with default settings (859). Fragments per kilobase million (FPKM) was used to quantify transcript expression levels. Analysis of differentially expressed genes (DEGs) was performed using DESeq2. Significant DEGs were identified with a P value < 0.05 and a $|\log_2(\text{fold change})| > 1$. KEGG enrichment analysis and gene set enrichment analysis (GSEA) were performed with clusterProfiler R package (860). The data reported in the present study have been deposited in the Gene Expression Omnibus (GEO) database under GEO accession number GSE211679.

2.13. RNA co-immunoprecipitation (RIP)

For RNA co-immunoprecipitations (RIP) cells (1×10^7 per condition) were cross-linked with 150 mJ/cm^2 using a UV crosslinker (Analytik

Jena, Germany) and then lysed on ice using RIP lysis buffer (50 mM Tris pH 8, 150 mM NaCl, 0.5% sodium deoxycholate, 1% Triton X-100, 5 mM MgCl2, 1 mM DTT, 1x proteinase inhibitor cocktail and 40U/mL RNase inhibitor). Anti-IGF2BP1-antibody or IgG were incubated with ProteinA/G magnetic beads (Beyotime) at 4 °C for 1 h. Cleared lysates were incubated with antibody-beads complexes at 4 °C overnight, followed by three washing steps with high salt buffer (50 mM Tris pH 8, 1 M NaCl, 1 mM EDTA, 1% NP-40, 0,5% sodium deoxycholate) and two washing steps with wash buffer (20 mM Tris pH 8, 150 mM NaCl, 0.5% NP-40), Protein enrichment was analyzed by western blotting. Co-purified RNAs were extracted using TRIZOL and analyzed by RT-qPCR.

2.14. Luciferase reporter assay

The 3′UTR of *MDM2* contains putative IGF2BP1 binding sites. Mutated 3′UTR of *MDM2* were synthesized using a QuikChange II XL Site-Directed Mutagenesis Kit (Stratagene), and the fragment was amplified by PCR. COV434 cells were co-transfected with the 3′UTR

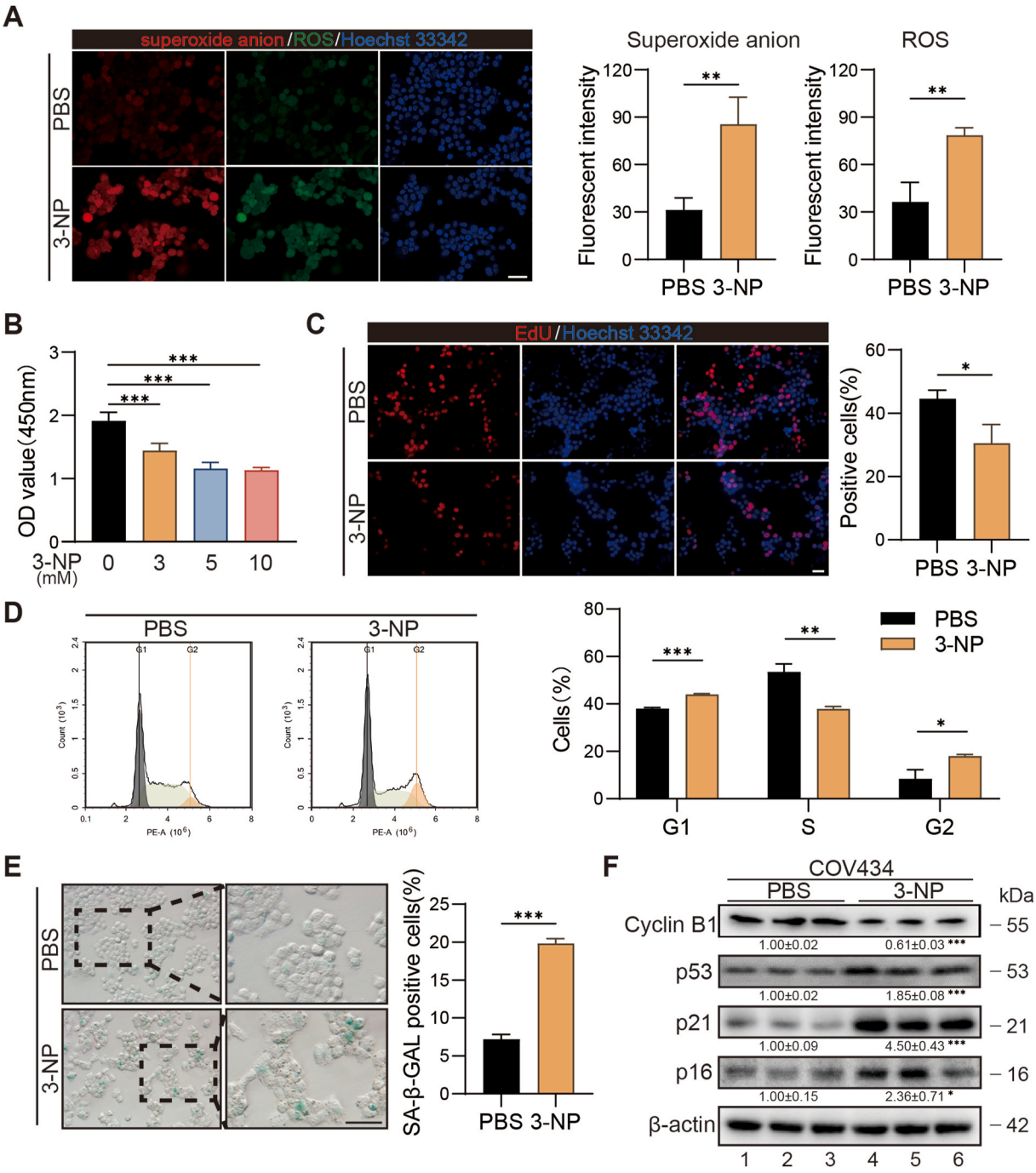

Fig. 1. 3-NP caused GCs dysfunction in vitro. (A) COV434 cells were treated with 10 mM 3-NP for 24h. Superoxide anion and ROS contents in control (PBS) or 3-NP treated (3-NP) cells were measured and quantified by measuring fluorescent intensity. (B) Cell viability changes after treatment with different concentrations of 3-NP were analyzed with CCK-8 assay. (C) Cell proliferation was determined by EdU assay and quantified by the percentage of positive cells. Representative images are shown in the left panel. (D) Cell cycle distribution analyses of control or 3-NP treated cells were analyzed with PI-labeled flow cytometry. (E) Cellular senescence levels were measured with SA-β-Gal staining and quantified by the percentage of positive cells. (F) Western blot analysis of indicated proteins in COV434 cells with or without 3-NP treatment. β-actin served as loading control. Bar: 50 μm *, $P < 0.05$; **, $P < 0.01$; ***, $P < 0.001$.

luciferase vector, pRL-TK and pcDNA3.1-IGF2BP1 using Lipofectamine 3000 (Invitrogen, USA). Renilla luciferase was used as internal reference. After 48 h of transfection, luciferase activities were measured using a Dual-Luciferase Reporter Assay System (Promega) following the manufacturer's instructions.

2.15. Statistical analysis

Statistical analyses were performed using GraphPad Prism 8.0 (version 8.0c; GraphPad Software, Inc., USA). All of the data were displayed as the mean ± SD and statistical significance of equally distributed data was tested by an unpaired parametric Student's t-test. Otherwise, a non-parametric Mann–Whitney-test was performed. Differences with P values < 0.05 were considered statistically significant.

3. Results

3.1. 3-NP caused GCs dysfunction in vitro

In this study, 3-NP, a mitochondrial toxin inducing OS by irreversibly inhibiting the succinate dehydrogenase enzyme in the complex II of electron transport chain, was used to simulate OS status of GCs both in vitro and in vivo. In agreement with the results acquired from other kinds of tissues such as the brain, liver and heart [34–36], 3-NP (10 mM) exposure resulted in massive ROS accumulation in granulosa cell line COV434 (Fig. 1A). Specifically, the level of superoxide anion, one of the major species of ROS, was also determined by dihydroethidium fluorescent probe and the result showed that the amount of superoxide anion also dramatically increased in 3-NP treated cells, suggesting the redox homeostasis was impaired in GCs after 3-NP treatment (Fig. 1A). We next tried to investigate the further impact of 3-NP on GCs. First, we performed CCK-8 and EdU assay to assess cell viability and proliferative ability respectively, finding that both cell viability and proliferation were obviously inhibited after 3-NP treatment (Fig. 1B and C). Given that previous studies have proved that the ROS level varies during the cell cycle progression [37] and can lead to cell cycle dysregulation [38, 39], we next determined the cell cycle phase distribution with flow cytometry. As seen in Fig. 1D, 3-NP treatment caused an obvious increase in the percentage of G1- or G2/M-phase cells, which reflected cell cycle arrest at the G1 and G2/M phase during the cell cycle progression. Since ROS are one of the stressors that may lead to senescence-associated phenotypes [40], we next evaluated the level of cellular senescence in GCs with or without 3-NP stimulation. The proportion of senescent cells, as determined by SA-β-Gal staining, was

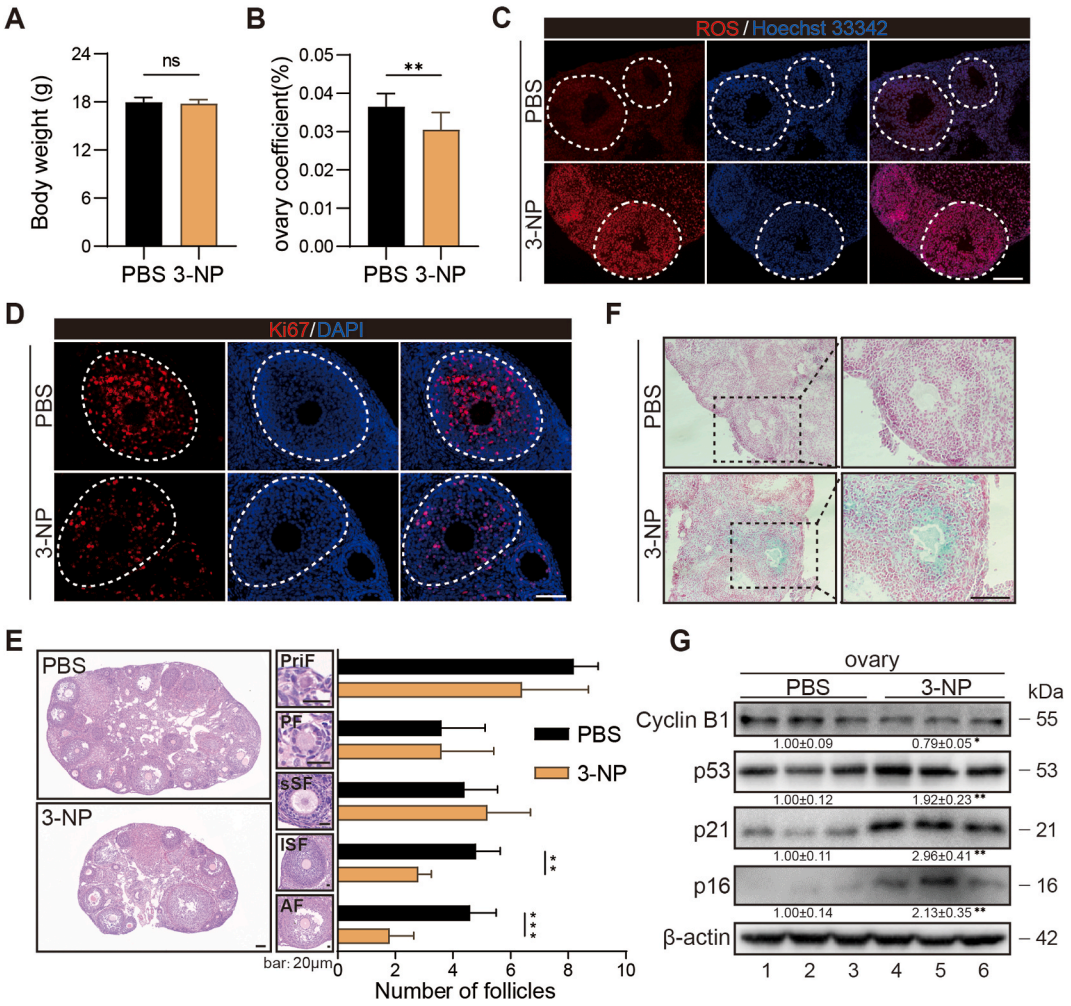

Fig. 2. 3-NP caused GCs dysfunction and impaired follicular development in C57BL/6J mice. (A, B) Body weights and ovary coefficients of C57BL/6J mice were recorded after 14 days of 3-NP/PBS intraperitoneal administration. (C) ROS levels of ovaries were measured. (D) Proliferative capacity of GCs was evaluated by detecting Ki-67, a marker of cell proliferation, with immunofluorescent staining. (E) Representative images of H&E staining showing ovarian histology and follicle morphology at different developmental stages. Follicle counts in ovaries of mice from the control or 3-NP group were analyzed. (F) Representative images of SA-β-Gal staining indicating senescent cells in ovaries. (G) Western blot analysis of indicated proteins in ovarian tissue. β-actin served as loading control. Bar: 100 μm ns, not statistically significant; *, $P < 0.05$; **, $P < 0.01$; ***, $P < 0.001$.

evidently increased in the 3-NP group, indicating a aggravated cellular senescent level (Fig. 1E). This result was further validated by Western blot analysis of several senescence-related markers, p16, p21, p53 and Cyclin B1 (Fig. 1F). Collectively, these data demonstrated that 3-NP treatment inhibited cell proliferation and exacerbated cellular senescence in GCs in vitro.

3.2. 3-NP caused GCs dysfunction and impaired follicular development in C57BL/6J mice

To further characterize the impact of 3-NP treatment on GCs, changes of mouse ovaries have been investigated in C57BL/6J mice. As shown in Fig. 2A and B, intraperitoneal administration of 3-NP did not result in significant changes on mouse body weights, but obviously decreased ovary coefficients (defined as ovary/body weight ratio), which reflected a global detrimental effect of 3-NP on mouse ovaries. To determine whether 3-NP administration resulted in a disturbed redox balance in vivo, DCFH-DA staining was performed to detect ROS levels of mouse ovaries. The intensive fluorescent signals manifested massive ROS accumulation in mouse ovaries, especially in GCs, of the 3-NP group (Fig. 2C), suggesting 3-NP stimulates an OS status in GCs in vivo as well. To further evaluate the 3-NP induced detrimental effect on mouse ovaries, we next analyzed the changes of pituitary hormone and sex hormone levels as the hormonal regulations within the HPG axis is crucial for maintaining normal folliculogenesis. The levels of estradiol, progesterone, follicle-stimulating hormone (FSH) and luteinizing hormone (LH) in mouse serum samples were measured by ELISA. The estradiol level in the 3-NP group was decreased compared to the control group whereas the level of progesterone was not obviously altered (Figs. S1A and B). Since the synthesis of estradiol is largely relied on intact GCs, decreased estradiol levels suggest the hormone synthesis function of GCs was impaired by 3-NP administration. FSH is a pituitary hormone that can stimulate estradiol secretion and is simultaneously modulated by estradiol levels through a feedback regulatory mechanism. The level of FSH elevated after 3-NP administration (Fig. S1C), which is consistent with the decreased level of estradiol. LH, another pituitary hormone promoting follicular development, was also modestly increased in mouse serum after 3-NP treatment, although this change was not significant (Fig. S1D). We next evaluated proliferative ability of GCs with Ki-67 IF staining. Comparing to the control group, the proportion of Ki-67 positive cells dramatically decreased in 3-NP treated mouse ovaries, indicating the proliferative capacity of GCs was impaired (Fig. 2D). GCs proliferation plays a pivotal role in follicular development, we then counted follicles at different stages in mice. As shown in Fig. 2E, the numbers of primordial, primary and small secondary follicles were not obviously affected, while the numbers of large secondary

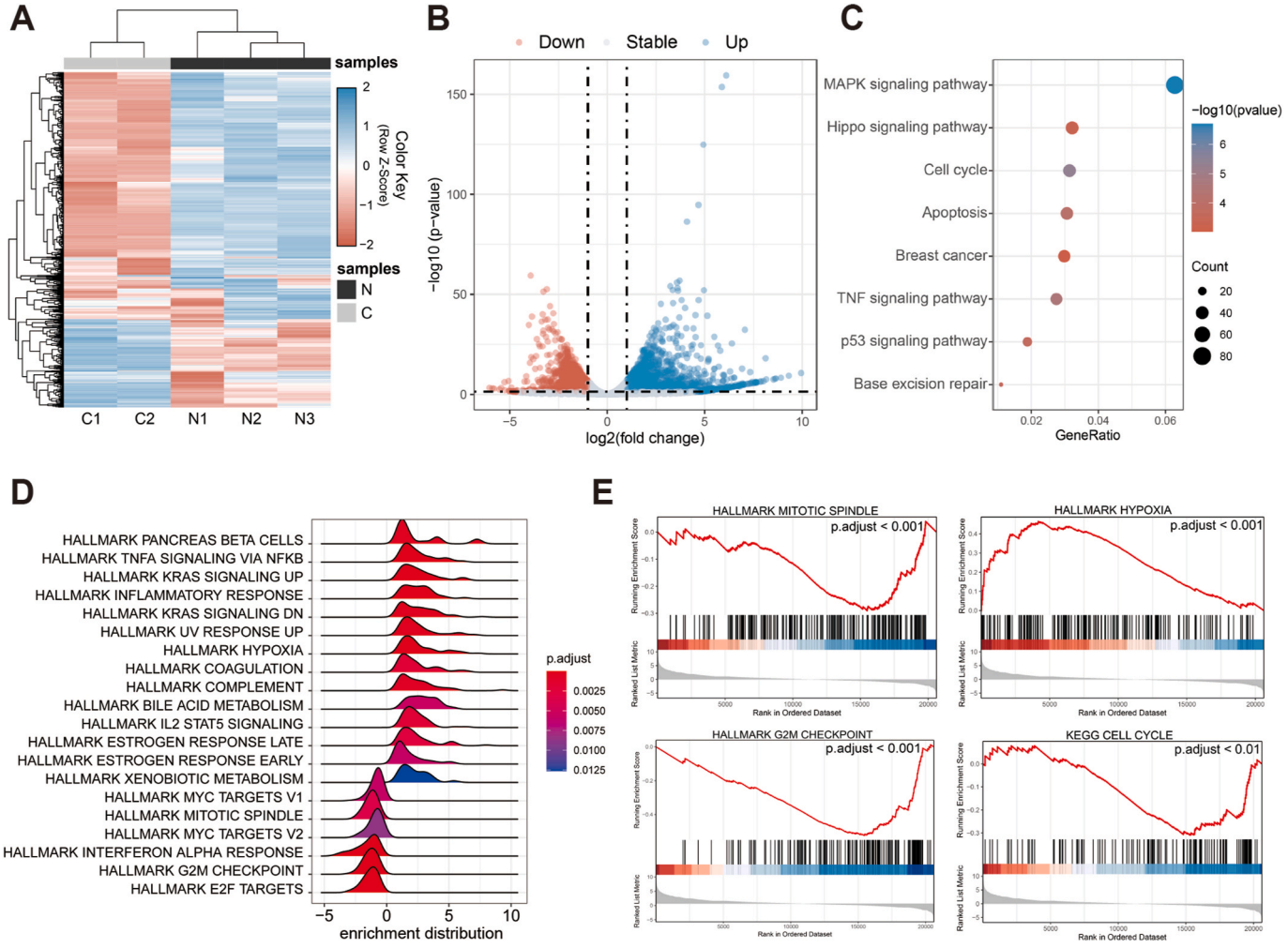

Fig. 3. Impact of 3-NP on global transcriptome profiling by RNA-seq. (A) Expression heatmap showing differential RNA-seq feature counts for COV434 cells with or without 3-NP treatment. This heatmap was built on normalized gene read counts. C = CONTROL; N = 3-NP. (B) Volcano plot obtained from DESeq2 analysis showing DEGs (|log2 fold change| $\geq$ 1 and $P < 0.01$) after 3-NP treatment. (C) KEGG pathway analysis of DEGs. GeneRatio is defined as (count of core enrichment genes)/(count of pathway genes). (D) The ridge plot visualizing the expression distributions of core enriched genes for GSEA enriched Hallmark gene sets. (E) GSEA results of the Hallmark pathway 'MITOTIC SPINDLE', 'HYPOXIA', 'G2M CHECKPOINT' and KEGG pathway 'Cell Cycle' are shown.

and antral follicles were significantly decreased in mice received 3-NP treatment, which further validated the declined proliferative ability of GCs. SA-β-Gal assay was then performed to determine the cellular senescent levels in mouse ovaries. As expected, strong SA-β-Gal staining was observed in the 3-NP group rather than the control group, illustrating an accumulation of senescent cells in ovarian follicles was induced by 3-NP treatment (Fig. 2F). Protein levels of p16, p21, p53 and Cyclin B1 also exhibited consistent changing trends (Fig. 2G), further indicating that 3-NP treatment caused aggravated cellular senescence in vivo as well. These results suggest that 3-NP exposure can also induce GCs dysfunction in vivo.

3.3. Impact of 3-NP on global transcriptome profiling by RNA-seq

Aiming to determine associated pathways and regulators involved in the process of 3-NP induced GCs dysfunction, we next performed RNA-seq in 3-NP treated COV434 cells. Comparative transcriptome analysis revealed the impact of 3-NP on global transcriptome, with the heatmap to visualize gene expression differences between 3-NP and control group (Fig. 3A). A total of 28,943 genes have been identified and analyzed, and 3538 genes were considered as differentially expressed genes ($|\log_2(\text{fold change})| > 1$ and adjusted p-value < 0.05 were set as the cut-off values), among which 1964 genes were upregulated and 1574 genes were downregulated, as shown in the volcano plot (Fig. 3B). The result of KEGG pathway enrichment analysis was illustrated by dot plot (Fig. 3C). Several enriched pathways, such as 'Cell cycle' and 'p53 signaling pathway', validated our previous findings that 3-NP treatment caused cell cycle disorder in GCs. In addition, GSEA was performed to further characterize transcriptome changes caused by 3-NP treatment. The ridge plot visualized expression distributions of core enriched genes in the enriched categories (Fig. 3D). Genes in several cell cycle associated gene sets, including 'HALLMARK MITOTIC SPINDLE', 'HALLMARK G2M CHECKPOINT' and 'KEGG CELL CYCLE', were mainly negatively regulated in 3-NP treated cells, whereas genes in the category of 'HALLMARK

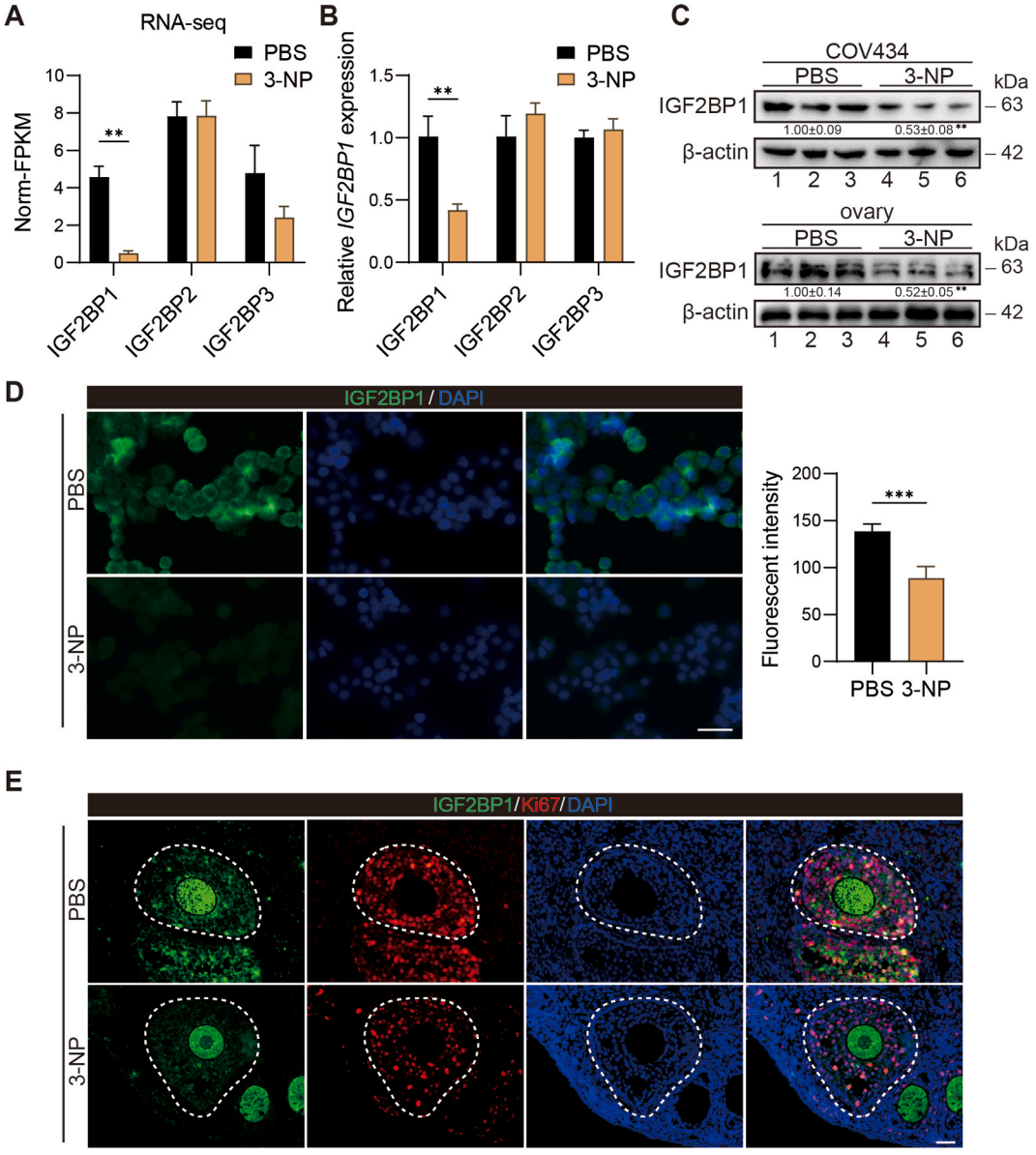

Fig. 4. 3-NP treatment downregulates IGF2BP1 in GCs. (A) Bar plots showing the expression levels of IGF2BPs in COV434 cells with or without 3-NP treatment. Data were derived from the RNA-seq and quantified by normalized FPKM. (B) RT-qPCR verification of RNA-seq results. (C) Western blot analysis of IGF2BP1 protein levels in COV434 cells (upper panel) and mouse ovaries (bottom panel). (D) Representative images of IGF2BP1 IF staining in COV434 cells. Relative quantification was performed using fluorescent intensity. (E) Representative images of IGF2BP1/Ki-67 double staining in ovarian slides. Bar: 50 μm **, $P < 0.01$; ***, $P < 0.001$.

HYPOXIA' showed an upregulated trend upon 3-NP treatment (Fig. 3E), providing an evidence for the 3-NP induced disturbance of redox homeostasis.

3.4. 3-NP treatment downregulates IGF2BP1 in GCs

We next try to identify the key regulator which is responsible for 3-NP induced GCs dysfunction. Having demonstrated that cell cycle dysregulation is one of the pivotal mechanisms underlying GCs damages, we reasoned that a cell cycle regulating factor might be involved in this process. Previous studies have revealed that IGF2BPs, an RNA-binding protein family facilitating to stabilize its target RNAs [15–18], play a key role in controlling cell cycle and regulating cancer cell proliferation [20,41–43]. IGF2BPs knockdown or depletion impaired cell cycle progression and limited tumor growth [20,41]. Intriguingly, IGF2BP1, rather than IGF2BP2 and IGF2BP3 was observed to be dramatically downregulated in 3-NP treated COV434 cells according to our RNA-seq data (Fig. 4A). In addition, the result of GSEA demonstrated the gene set 'HALLMARK E2F TARGETS' was enriched and mainly negatively regulated in 3-NP treated cells (Fig. 3D). It has been revealed that IGF2BP1 is a post-transcriptional enhancer of E2F-driven gene expression and IGF2BP1 depletion led to significant downregulation of E2F-driven genes [20]. These results are consistent with our data and suggest IGF2BP1 may serve as part of the regulatory mechanism underlying 3-NP-induced GCs dysfunction.

To validate this result, we performed RT-qPCR and Western blot to evaluate the mRNA and protein levels of IGF2BP1. It was found that both mRNA and protein levels were obviously decreased after 3-NP treatment (Fig. 4B and C). In addition, IF staining of IGF2BP1 was performed in COV434 cells. The fluorescence signal distribution revealed the cytoplasmic localization of IGF2BP1, and the fluorescent intensity was obviously decreased in the 3-NP group, further confirming that 3-NP treatment inhibited IGF2BP1 expression in GCs (Fig. 4D). Since 3-NP induced mitochondrial dysfunctions not only lead to increased ROS generation, but also to the impairment of ATP production, we next investigated whether the IGF2BP1 downregulation in GCs is due to excessive ROS or energy depletion. Aside from 3-NP, we used antimycin A (an inhibitor of mitochondrial electron transport chain complex III), FCCP (a mitochondrial oxidative phosphorylation uncoupler) and H_2O_2 to treat COV434 cells and measured the changes of ROS levels, intracellular ATP contents and IGF2BP1 expression levels upon these different treatments. As shown in Figure S2A, S2B and S2C, exposure to 3-NP and H_2O_2 significantly elevated ROS levels but only moderately decreased intracellular ATP production. FCCP treatment resulted in a drastic decrease in ATP contents but ROS elevation was relatively mild in FCCP-treated cells, whereas antimycin A caused pronounced changes in both ROS and ATP levels. IGF2BP1 expression has been inhibited to varying degrees by all these four treatments. The differences between H_2O_2 group and 3-NP/Antimycin A group suggest that IGF2BP1 expression is under regulation of both ROS and ATP levels, whereas the difference between the 3-NP and FCCP group indicates that GCs may be more sensitive to ROS elevation than to ATP reduction in terms of IGF2BP1 expression (Fig. S2D). This hypothesis was further validated by the result of pretreatment of NAC, an ROS scavenger, partially reversing 3-NP induced IGF2BP1 downregulation (Fig. S2D, lane8 vs 7). However, how and to what extent IGF2BP1 expression is modulated by those ROS-independent cellular disorders need further exploration. In addition, we measured the changes of IGF2BP1 levels upon 3-NP exposure in KGN and HEK293T cell lines. Both immunofluorescent staining and Western blot demonstrated that IGF2BP1 expression was decreased after 3-NP treatment in KGN cells (Figs. S2E and F) as well as in HEK293T cells, but in a much slighter degree (Figs. S2G and H), suggesting that 3-NP induced IGF2BP1 downregulation is not a GCs-specific response.

Furthermore, IGF2BP1 downregulation upon 3-NP treatment was also observed in vivo. Western blot analysis demonstrated dramatically decreased IGF2BP1 protein levels in ovaries of 3-NP administered mice (Fig. 4C). IF staining validated this result. As shown in Fig. 4E, intensive IGF2BP1 fluorescent signals were detected in both GCs and oocytes of the control group. While in 3-NP treated mice, the fluorescent intensity in ovaries was generally decreased, and the decline in GCs was much more obvious than that in oocytes, suggesting 3-NP treatment can lead to IGF2BP1 downregulation in GCs both in vitro and in vivo.

3.5. IGF2BP1 regulates cell proliferation, cell cycle and cellular senescence in GCs

We next investigate the effects of IGF2BP1 in GCs through loss- and gain-of-function experiments. IGF2BP1 was silenced or overexpressed by using IGF2BP1-directed siRNA or pcDNA3.1-IGF2BP1 plasmids respectively. The silencing and overexpression efficiency were validated by RT-qPCR and western blotting (Figs. S3A and B). As expected, CCK-8 assay indicated that cell viability was significantly impaired by IGF2BP1 knockdown at 72 h post-transfection (Fig. 5A). Cell proliferative capacity was evaluated by EdU assay. The decreased proportion of EdU-positive cells validated the inhibited cell proliferation upon IGF2BP1 silencing (Fig. 5C). In contrast, ectopically expressed IGF2BP1 facilitated GCs proliferation and enhanced GCs viability as early as 24 h post-transfection (Fig. 5B, D). We next performed flow cytometry to analyze the impact of IGF2BP1 silencing or overexpression on cell cycle distribution. As shown in Fig. 5E, IGF2BP1 knockdown impaired G1/S transition and increased the proportion of cells in G2/M phase, whereas IGF2BP1 overexpression facilitated G1/S transition, but did not significantly affected the proportion of G2/M cells (Fig. 5F), indicating IGF2BP1 is involved in maintaining normal cell cycle progression in GCs. Given that cell cycle arrest, which has been observed in IGF2BP1-depleted GCs, is one of the hallmarks of senescent phenotypes [44], we next investigated whether IGF2BP1 expression affects cellular senescence in GCs. As shown in Fig. 5G, IGF2BP1 knockdown obviously increased the percentage of SA-β-Gal-positive cells, whereas IGF2BP1 overexpression resulted in relatively light staining, but did not significantly affect the positive rate (Fig. 5H). We further strengthen this conclusion by determining the protein levels of senescence-associated markers. As expected, expression of p16, p21 and p53 was enhanced after IGF2BP1 knockdown and inhibited after IGF2BP1 overexpression while the level of Cyclin B1 exhibited an opposite trend in response to IGF2BP1 silencing or overexpression (Fig. 5I). These findings suggest that IGF2BP1 is involved in regulating GCs proliferation, cell cycle and cellular senescence. Furthermore, IGF2BP1 knockdown inflicted a 3-NP-simialr effect on GCs, indicating IGF2BP1 downregulation may be partially responsible for 3-NP induced GCs dysfunction.

3.6. IGF2BP1 rescues 3-NP induced GCs dysfunction

To further investigate if the adverse effects of 3-NP on GCs are at least partially mediated by IGF2BP1 downregulation, we next examined if ectopically expressed IGF2BP1 could restore part of the GCs functions hindered by 3-NP treatment. GCs were treated with 3-NP in the presence of ectopically expressed IGF2BP1 or vehicle control, after which the protein level of IGF2BP1 was validated by Western blot (Fig. 6E). As illustrated in Fig. 5A, the result of CCK-8 and EdU assay demonstrated that the impaired GCs viability and proliferative capacity were partially reversed by IGF2BP1 overexpression (Fig. 6A and B). We next examined whether 3-NP induced cell cycle disorders can also be corrected by ectopically expressed IGF2BP1. As shown in Fig. 5E, the elevated proportion of G1- and G2/M-phase cells was obviously deceased in the IGF2BP1 overexpressed cells, indicating IGF2BP1 restoration facilitated cell cycle progression (Fig. 6C). In accordance with these results, the number of senescent cells, which was dramatically increased after 3-NP exposure, exhibited an obvious downward trend in IGF2BP1-overexpression group (Fig. 6D). Furthermore, protein levels of senescent markers validated the result of SA-β-GAL assay, with p16, p21, p53 inhibited and Cyclin B1 rebounded after IGF2BP1 overexpression

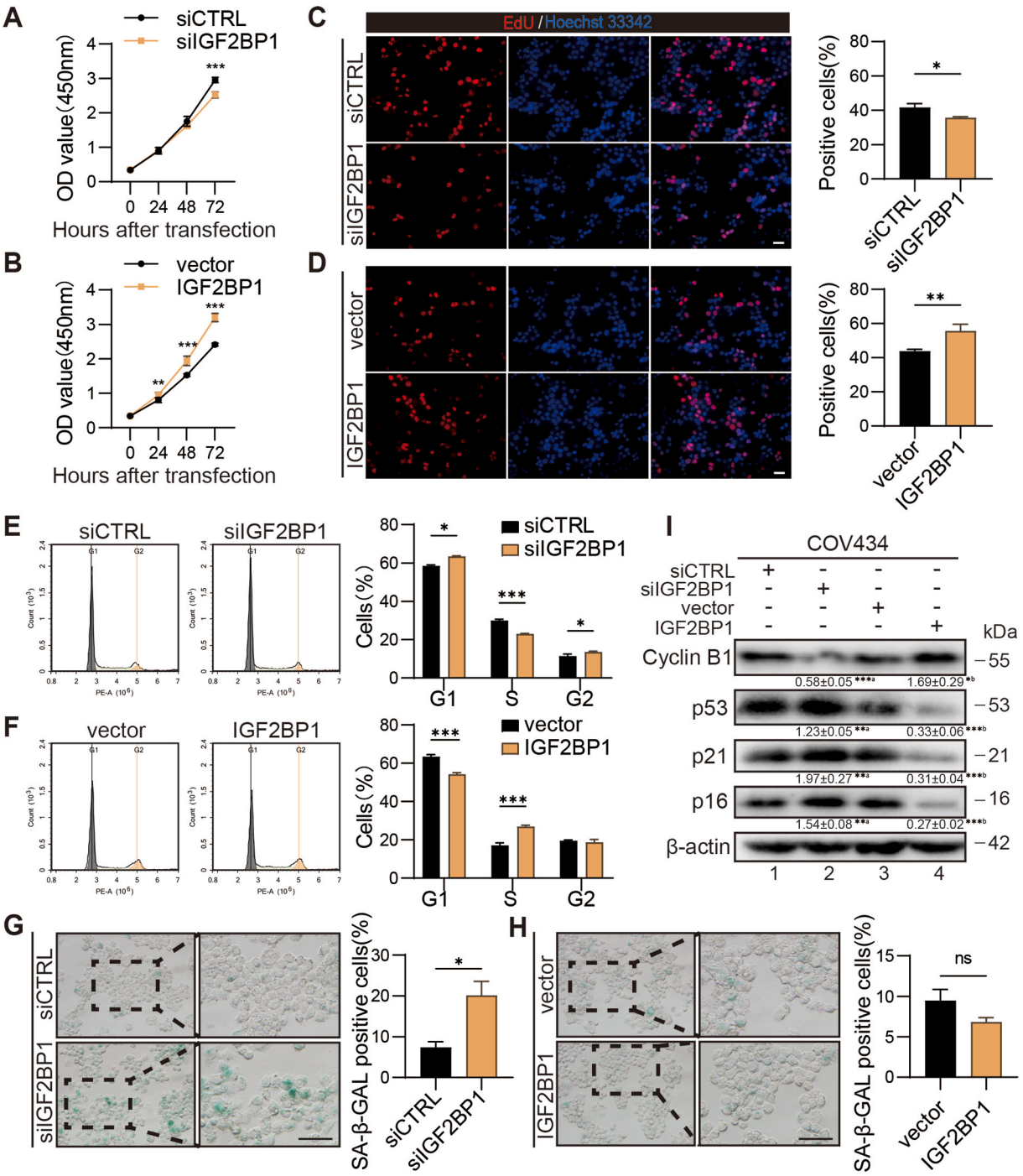

Fig. 5. IGF2BP1 regulates cell proliferation, cell cycle and cellular senescence in GCs. (A, B) COV434 cells were transfected with control/IGF2BP1-directed siRNA (siCTRL/siIGF2BP1) or pcDNA3.1-vector/pcDNA3.1-IGF2BP1 (vector/IGF2BP1). Cell viability changes were measured 24/48/72h after transfection. (C, D) Cell proliferative capacity was determined by EdU assay and quantified by the percentage of positive cells. (E, F) Cell cycle distribution changes upon IGF2BP1 knockdown or overexpression were analyzed with PI-labeled flow cytometry. (G, H) Cellular senescence levels were measured with SA-β-Gal staining and quantified by the percentage of positive cells. (I) Representative Western blot analysis of indicated proteins in COV434 cells after IGF2BP1 knockdown of overexpression. β-actin was used as loading control. a, lane1 vs 2; b, lane3 vs 4. Bar: 50 μm ns, not statistically significant; *, $P < 0.05$; **, $P < 0.01$; ***, $P < 0.001$.

(Fig. 6E). These findings suggest that IGF2BP1 overexpression partially alleviates 3-NP induced GCs dysfunction and IGF2BP1 downregulation meditates part of the 3-NP induced GCs damages.

3.7. *IGF2BP1 recognizes and regulates MDM2 in an m^{6}A-dependent manner*

Having demonstrated that IGF2BP1 is one of the potential effectors during 3-NP induced GCs dysfunction, we next aimed to reveal which factor is responsible for the detrimental impact meditated by IGF2BP1 downregulation. Given that IGF2BP1's main and conserved role in cancer-derived cells relies on the 3′UTR- and m^{6}A-dependent regulation of mRNA stability [20,45], we reasoned that IGF2BP1's involvement in 3-NP induced GCs dysfunction might also be associated with its property as an RNA binding protein. We combined differentially expressed genes identified by RNA-seq (performed in COV434 cells with or without 3-NP

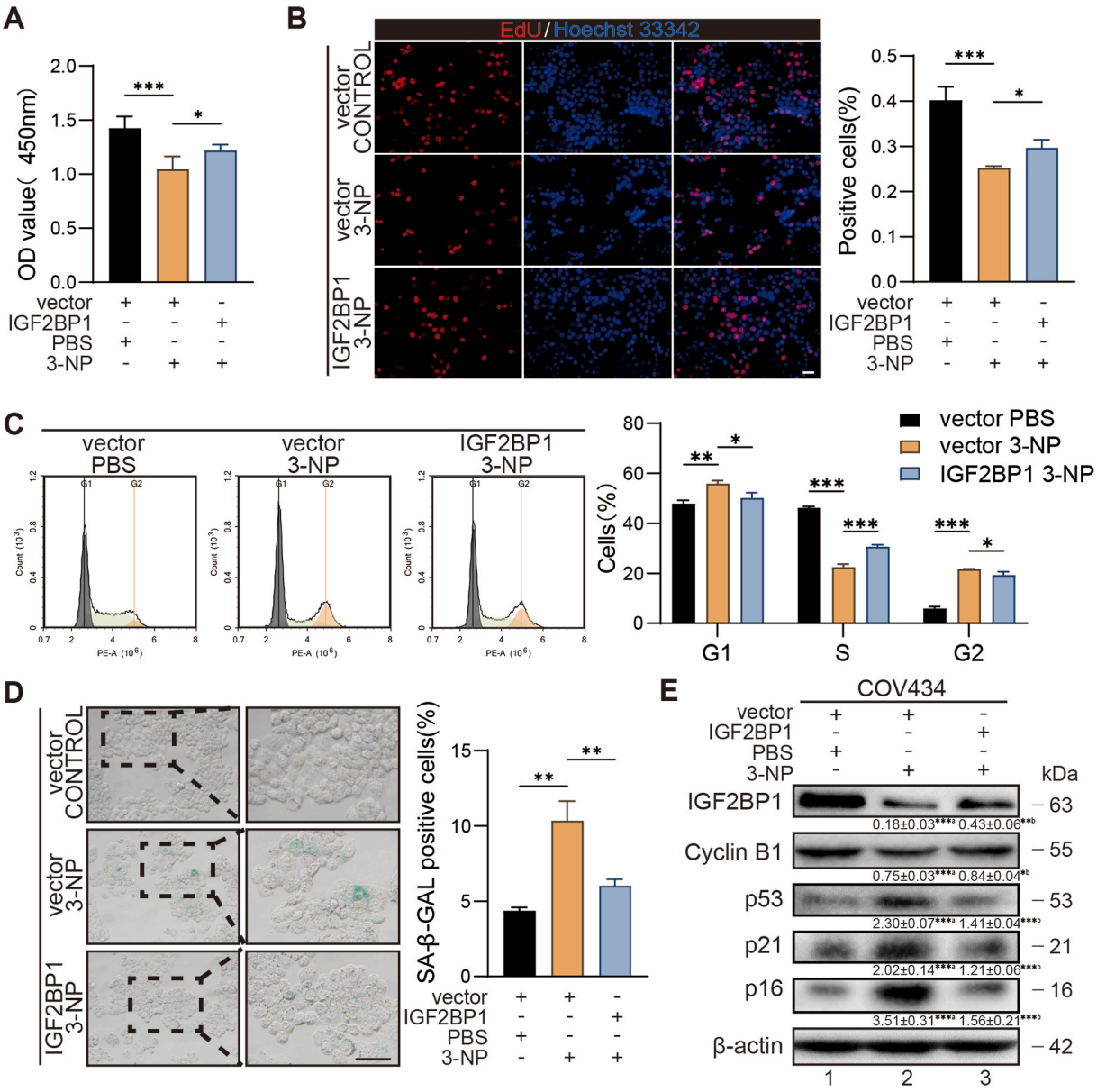

Fig. 6. IGF2BP1 rescues 3-NP induced GCs dysfunction. (A) COV434 cells were transfected with pcDNA3.1-vector or pcDNA3.1-IGF2BP1, 3-NP was added to the medium 48h after transfection. Cell viability was measured 24h after 3-NP treatment. (B) Cell proliferation was analyzed by EdU assay and quantified with the percentage of positive cells. (C) Cell cycle distribution changes were analyzed with PI-labeled flow cytometry. (D) Senescent cells were indicated with SA-β-Gal staining. (E) Representative Western blot analysis of indicated proteins in COV434 cells. β-actin served as loading control. a, lane1 vs 2; b, lane2 vs 3. Bar: 50 μm *, $P < 0.05$; **, $P < 0.01$; ***, $P < 0.001$.

treatment) and IGF2BP1-binding transcripts profiled by RNA immunoprecipitation sequencing (RIP-seq, GSE90639), 601 genes were found in the intersection of these two gene lists (Fig. 7A). KEGG pathway enrichment analysis was performed to further screen the possible targeted mRNAs. As a result, several pathways such as 'Cell cycle' and 'Cellular senescence', which are highly consistent with GCs changes after 3-NP treatment or IGF2BP1 knockdown, were enriched (Fig. 7B). Since both the p53 and FoxO signaling pathways are also important in regulating cell cycle and cellular senescence, we obtained the overlapping elements among these four pathways, eventually MDM2, together with two other genes encoding the Cyclin proteins, was shortlisted for the possible IGF2BP1 targets (Fig. 7C).

We next examined the mRNA and protein levels of MDM2 after 3-NP treatment and IGF2BP1 knockdown/overexpression. As expected, MDM2 was downregulated in 3-NP treated and IGF2BP1-knockdowned cells, and upregulated in IGF2BP1 overexpression cells (Fig. 7D and E). Furthermore, the effect of IGF2BP1 expression alteration on *MDM2* mRNA stability was investigated by the Actinomycin D (ActD) chase experiment. Forty-eight hours after the transfection, 5 μg/mL ActD was added to the medium and total RNA was collected 0, 3 and 6h after ActD administration. As shown in Fig. 7F, IGF2BP1 knockdown and ectopic expression resulted in the impaired and enhanced stability of *MDM2* mRNA respectively, further validating the role of IGF2BP1 in mRNA metabolism. In view of IGF2BP1 had been identified as an m^6A reader recognizing and binding transcripts with m^6A modifications, we explored whether m^6A modifications are essential for IGF2BP1-*MDM2* interaction in GCs. The m^6A sites of *MDM2* mRNA were predicted by SRAMP database [46] and further validated by MeRIP-seq (GSE178095), while the IGF2BP1-binding sites were determined by RIP-seq (GSE90639). It was found that m^6A sites and IGF2BP1-binding sites highly overlapped and were both enriched around the stop codon and 3′UTR of *MDM2* mRNA, suggesting IGF2BP1 might recognize and

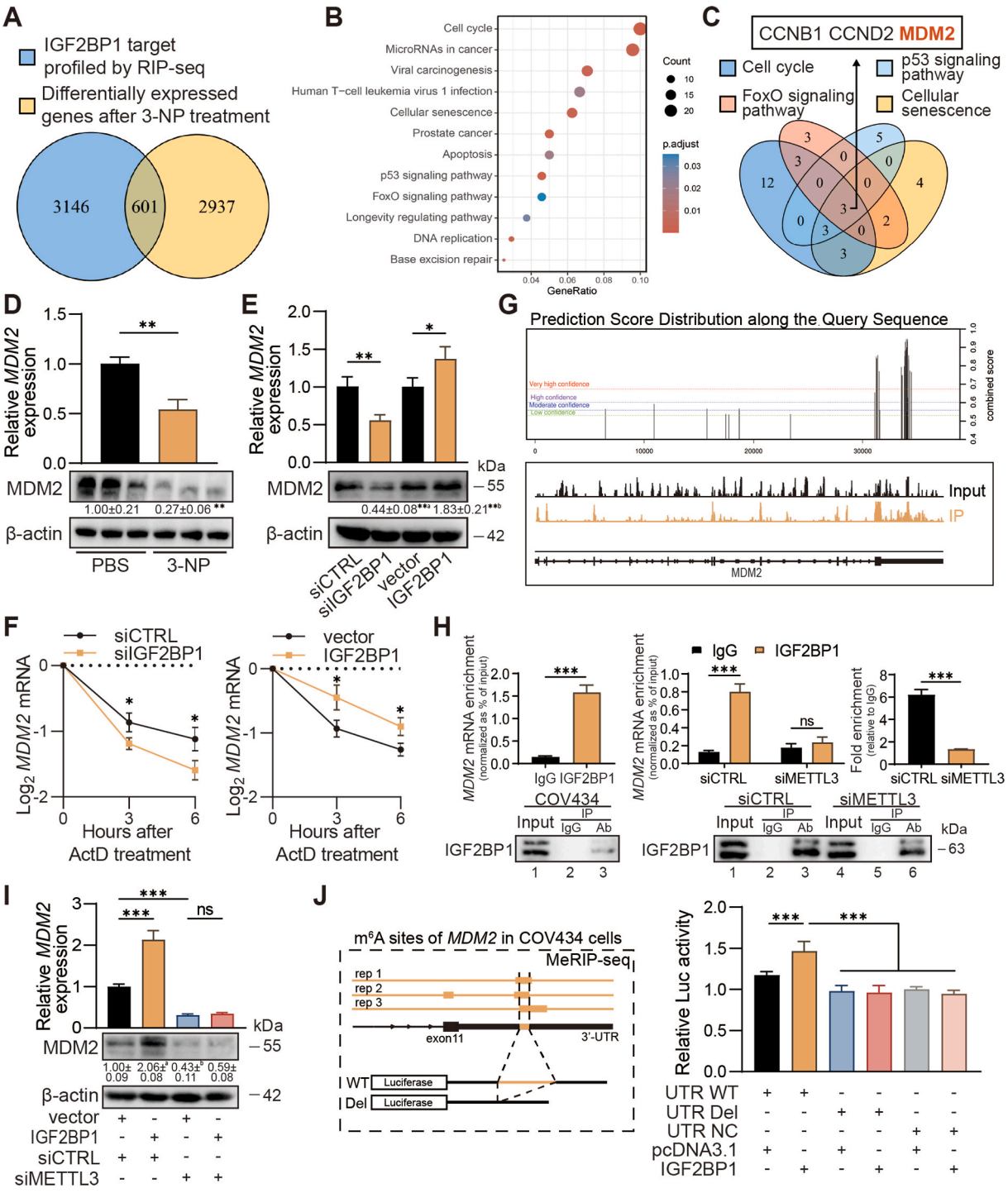

Fig. 7. IGF2BP1 recognizes and regulates *MDM2* mRNA in an m^{6}A-dependent manner. (A) Venn diagram showing the intersection of DEGs from RNA-seq and enriched transcripts from IGF2BP1 RIP-seq. (B) KEGG pathway enrichment analysis of genes obtained from the intersection. (C) Venn diagram showing the intersection of KEGG pathway 'Cell cycle', 'p53 signaling pathway', 'FoxO signaling pathway' and 'Cellular senescence'. (D, E) RT-qPCR and Western blot analysis of mRNA and protein levels of MDM2 in COV434 cells after 3-NP treatment and IGF2BP1 knockdown/overexpression. a, lane1 vs 2; b, lane3 vs 4; (F) RT-qPCR analysis of *MDM2* mRNA levels 0/3/6h after ActD treatment in IGF2BP1 depleted/overexpressed COV434 cells. (G) Map of SRAMP-predicted m^{6}A sites and IGF2BP1-RIP peaks on MDM2 mRNA. (H) Co-purification of MDM2 mRNAs with IGF2BP1 in wildtype, control- (siCTRL) or METTL3-depleted(siMETTL3) COV434 cells was analyzed by RIP using anti-IGF2BP1 antibodies and RT-qPCR analysis. (I) RT-qPCR and Western blot analysis of mRNA and protein levels of MDM2 in COV434 cells after IGF2BP1 overexpression and/or METTL3 knockdown. a, lane2 vs 1, $P < 0.001$; b, lane3 vs 1, $P < 0.01$. (J) Schematic representation showing the reporters harboring wildtype or m^{6}A-enriched-region deleted fragments of SOX2-3′UTR (left panel). Dual luciferase reporter analysis of MDM2-3′UTR-driven firefly luciferase reporter constructs in COV434 cells with ectopically expressed IGF2BP1 (right panel). ns, not statistically significant; *, $P < 0.05$; **, $P < 0.01$; ***, $P < 0.001$.

regulate *MDM2* mRNA in an m^{6}A-dependent manner (Fig. 7G). We next performed IGF2BP1 RIP assay in WT and METTL3-knockdown cells to validate this hypothesis. Given that METTL3 serves as a key component of m^{6}A methyltransferase complex, METTL3 knockdown (Fig. S3C) will significantly decreases m^{6}A levels of the whole transcriptome, thus hampering the interaction between m^{6}A readers and their target transcripts. As it turned out, the interaction between IGF2BP1 and *MDM2* mRNA, which was evidenced by RIP assay performed in WT cells, was obviously impeded by METTL3 knockdown (Fig. 7H). This result was further strengthened by changes of the MDM2 protein level in response to METTL3 knockdown. As depicted in Fig. 7I, MDM2 expression was respectively enhanced and suppressed after IGF2BP1 overexpression (lane2 vs 1) and METTL3 knockdown (lane3 vs 1), and the IGF2BP1 meditated *MDM2* upregulation was largely attenuated by METTL3 inhibition (lane4 vs 3). We next expected to test whether the presence of the m^{6}A-harboring fragment is required for IGF2BP1 binding to *MDM2*-3′UTR. Luciferase reporter constructs harboring either wildtype or mutant (containing deletion of the m^{6}A enriched region defined by

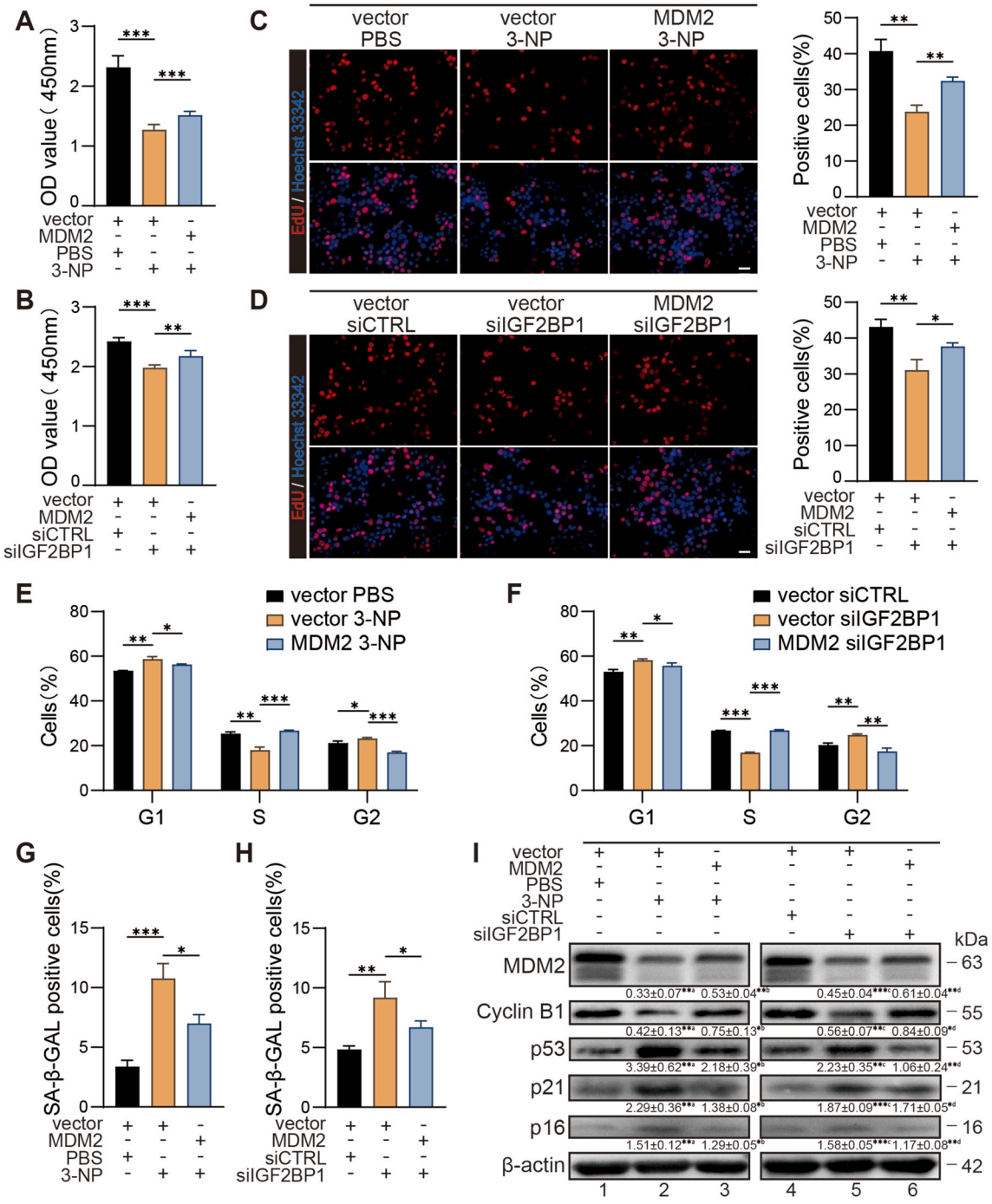

Fig. 8. MDM2 rescues 3-NP or IGF2BP1-knockdown induced GCs dysfunction. (A, B) 3-NP treated or IGF2BP1-depleted COV434 cells were transfected with pCMV-vector or pCMV-MDM2. Cell viability was measured with CCK-8 assay. (C, D) Cell proliferation was analyzed by EdU assay and quantified with the percentage of EdU-positive cells. Representative images were shown in the left panel. (E, F) Cell cycle phase distribution was determined by PI-labeled flow cytometry. (G, H) Cellular senescence was quantified by the percentage of SA-β-Gal-positive cells. (I) Representative Western blot analysis of indicated proteins in COV434 cells. β-actin served as loading control. a, lane1 vs 2; b, lane2 vs 3, c, lane4 vs 5; d, lane5 vs 6. Bar: 50 μm *, $P < 0.05$; **, $P < 0.01$; ***, $P < 0.001$.

MeRIP-seq) fragment of *MDM2*-3′UTR were generated, as shown in Fig. 7J (left panel). Overexpression of IGF2BP1 induced a significant increase in luciferase activity in cells transfected with WT reporter harboring wildtype 3′UTR of *MDM2* mRNA, but such elevation was impaired by deletion of the m^6A enriched region of the reporter (Fig. 7J, right panel). Taken together, these results indicated that the m^6A modifications on *MDM2*-3′UTR are indispensable for IGF2BP1 recognizing and binding to 3′UTR region, thus regulating *MDM2* mRNA stability in damaged GCs.

3.8. MDM2 rescues GCs dysfunction induced by 3-NP or IGF2BP1 knockdown

To explore whether MDM2 inhibition partially mediates the GCs dysfunction induced by 3-NP treatment and IGF2BP1 downregulation, we observed the effect of MDM2 overexpression on GCs functions in damaged GCs. The overexpression efficiency was verified by RT-qPCR and Western blot (Fig. S3D). The COV434 cells were transfected with pCMV-MDM2 plasmids either in the presence of IGF2BP1-directed siRNA or followed by 3-NP treatment, and the evaluation of cell functions was performed as described previously. Both cell viability and cell proliferative capacity, which were impaired by 3-NP treatment and IGF2BP1 knockdown, have been efficiently rescued after MDM2 overexpression (Fig. 8A, B, C, D). As expected, since MDM2 has already been identified as a pivotal factor in cell cycle regulation, its overexpression also facilitated the cell cycle progression in both 3-NP treated or IGF2BP1 knockdown cells (Fig. 8E, F, Figs. S4A and B). We next examined whether ectopically expressed MDM2 alleviated cellular senescence via performing SA-β-Gal assay and measuring protein levels of senescence-associated markers, finding that MDM2 supplement significantly reduced the number of senescent cells (Fig. 8G, H, Figs. S4C and D)and resulted in partial recovery of protein levels of senescence-related hallmarks (Fig. 8I). These results further validated the hypothesis that IGF2BP1 plays a role in regulating GCs function by maintaining the stability of *MDM2* mRNA, which uncovers a novel molecular regulatory mechanism underlying the OS-related GCs dysfunction and subsequent ovarian follicular developmental disorder.

4. Discussion

Serving as the supporting somatic cells in follicles, proliferating GCs control the progression of folliculogenesis and provide the microenvironment required for the acquisition of a meiotically competent oocyte [47,48]. GCs dysfunction has been proved to be involved in various female reproductive diseases [49–51], thus making detrimental impact on female fertility. OS is one the culprits of GCs dysfunction. The imbalance between oxidants and antioxidants brings about broad-ranging and significant effects on cells, leading to impaired proliferation, increased apoptosis and abnormal cell cycle progression [52,53]. Several studies have revealed the negative implications of OS on GCs [13,54,55], the molecular mechanisms underlying which, however, still remain unclear.

Here, we observed the impact of 3-NP, a mitochondrial toxin targeting complex II of electron transport chain and inducing various mitochondria-related disorders, on GCs both in vitro and in vivo. Similar to previous studies, GCs exhibited limited proliferative capacity and exacerbated cellular senescence following 3-NP exposure. In consequence, 3-NP induced GCs dysfunction resulted in follicular development disorder and may be responsible, as least partially, for the ovary coefficient reduction in mice. Considering OS is such a common phenomenon that participates in kinds of female reproductive diseases, whether and how GCs dysfunction regulates the progression of these diseases and subsequent fertility loss worth further exploration.

IGF2BP1, an RNA binding protein enhancing the stability of its target transcripts, has been found to be significantly downregulated after 3-NP treatment and may serve as a pivotal regulator meditating OS associated GCs dysfunction. The conserved proliferation-stimulating role of IGF2BP1 has been evidenced by massive studies in various kinds of cancers. This cancer-promoting effect is largely relied on its m^6A-dependent stabilization of several oncogene mRNAs [20,56,57]. However, the evidences revealing the role of IGF2BP1 in non-cancer cells are much more limited. Manieri et al. found that IGF2BP1 functions as a key regulator of colonic injury and repair by facilitating the induction of Ptgs2 mRNA in colonic mesenchymal stem cells [58]. While in immune thrombocytopenia, IGF2BP1 is involved in regulating apoptosis of mesenchymal stem cells [22]. Comparing to its cancer-related effect, the role of IGF2BP1 in normal cells has been rarely investigated and to be more specific, the participation of IGF2BP1 in OS or female reproductive diseases has not been unveiled yet. Our studies indicate 3-NP treatment induced dramatic IGF2BP1 downregulation partially by stimulating ROS overproduction. The depletion of IGF2BP1 in GCs impairs cell viability, restrains cell proliferation, hinders cell cycle progression and aggravates cellular senescence. In contrast, IGF2BP1 overexpression results in the opposite effects in GCs and partially rescues 3-NP induced GCs dysfunction. These results further validated the pro-proliferative effect of IGF2BP1, which revealed another key regulator of OS-associated cell damage and broadened the range of cell types where IGF2BP1 plays a role in regulating cell cycle. Given that GCs proliferation is required for follicular development and oocyte maturation, whether and how much the level of IGF2BP1 in GCs varies in female reproductive diseases need more investigation. In addition, further evidences are needed to understand the specific impact of IGF2BP1 on the whole transcriptome scale and other aspects of cell behaviors in GCs.

Previous studies have demonstrated that IGF2BP1 is an RBP which functions by enhancing the stability of its targeted transcripts, so we next explored the possible downstream mRNAs that is regulated by IGF2BP1 and responsible for the IGF2BP1-mediated GCs dysfunction. We combined results of RNA-seq performed in COV434 cells (with or without 3-NP treatment) and IGF2BP1 RIP-seq, eventually MDM2 was identified as the IGF2BP1 target. In accordance with previous studies, IGF2BP1 acts as a post-transcriptional enhancer of MDM2 expression, increasing its mRNA stability and subsequent protein expression. One of the crucial observations of our study is that IGF2BP1-controlled MDM2 expression is apparently m^6A-dependent. IGF2BP1 binding sites and m^6A modification sites are highly overlapping and peaking around 3′UTR of *MDM2* mRNA, which is consistent with previously reported m^6A-enriched regions [59,60]. Furthermore, the knockdown of METTL3, an essential catalytic subunit required for methyltransferase activity, significantly repressed IGF2BP1-*MDM2* interaction in GCs. This emphasizes and further validates the recently reported m^6A reader role of IGF2BP1.

MDM2 is an E3 ligase for p53 and for itself. In cancer cells, it inhibits p53 activity in several pathways, thus promoting cell cycle progression and uncontrolled cell proliferation [61]. Our results indicate that *MDM2* is under the m^6A-dependent and post-transcriptional control of IGF2BP1 in GCs. MDM2 partially meditates IGF2BP1-directed proliferating-stimulating effect. Overexpression of MDM2 facilitates cell cycle phase transition and alleviates cellular senescence induced by 3-NP treatment and IGF2BP1 knockdown. These findings expand the pro-proliferating role of MDM2 and strongly suggest that METTL3-catalyzed m^6A modification is a conserved and indispensable mechanism for cell cycle progression in both caner and non-cancer cells.

GCs dysfunction is a pathological condition that can be found in a variety of female reproductive diseases. Multi-source detrimental factors from these diseases inflict damages on GCs, contributing to steroidogenesis disorder, folliculogenesis disarrangement and oocyte incompetence, ultimately resulting in infertility [31,62]. Therefore, unveiling the molecular regulatory network meditating GCs dysfunction can be helpful in interpreting and further analyzing those GCs-related pathological phenomena and clinical manifestations. This study has focused on clarifying the role of IGF2BP1 in 3-NP induced GCs damages. However, the effect of IGF2BP1 knockdown or overexpression on cell

viability, proliferation, cell cycle and cellular senescent levels was also explored in normal GCs, which partially demonstrated the regulatory effect of IGF2BP1 on GCs behaviors and functions, including but not limited to the OS condition. Given that fully functional GCs are indispensable for normal follicular development, these findings provide a novel potential clinical marker for predicting the GCs status as well as the follicular developmental potential, which, however, requires further researches to reveal the in vivo effect of IGF2BP1 on GCs.

5. Conclusion

In summary, this study elucidated the critical role of IGF2BP1 in regulating 3-NP induced GCs damages. We revealed IGF2BP1 is essential for maintaining normal cell cycle progression and proliferation in GCs by enhancing *MDM2* mRNA stability in an m^6A-dependant manner. Our present study provides insights into the biological function of IGF2BP1 in modulating GCs growth and follicular development, which provides evidences for taking IGF2BP1 as a novel therapeutic target in tackling OS induced ovarian dysfunction.

Funding

This work was supported by National Natural Science Foundation of China (92068120) and The Key R&D Program of Hubei Province (2022BCB024).

Declaration of competing interest

The authors declare that they have no known competing financial interests or personal relationships that could have appeared to influence the work reported in this paper.

Data availability

The data reported in the present study have been deposited in the Gene Expression Omnibus (GEO) database.

Appendix A. Supplementary data

Supplementary data to this article can be found online at https://doi.org/10.1016/j.redox.2022.102492.

References

[1] L. Schmidt, T. Sobotka, J.G. Bentzen, A. Nyboe Andersen, Demographic and medical consequences of the postponement of parenthood, Hum. Reprod. Update 18 (2012) 29–43, https://doi.org/10.1093/humupd/dmr040.
[2] J. Bellver, J. Donnez, Introduction: infertility etiology and offspring health, Fertil. Steril. 111 (2019) 1033–1035, https://doi.org/10.1016/j.fertnstert.2019.04.043.
[3] Q. Li, X. Geng, W. Zheng, et al., Current understanding of ovarian aging, Sci. China Life Sci. 55 (2012) 659–669, https://doi.org/10.1007/s11427-012-4352-5.
[4] M. Hayyan, M.A. Hashim, I.M. AlNashef, Superoxide ion: generation and chemical implications, Chem. Rev. 116 (2016) 3029–3085, https://doi.org/10.1021/acs.chemrev.5b00407.
[5] B. D'Autréaux, M.B. Toledano, ROS as signalling molecules: mechanisms that generate specificity in ROS homeostasis, Nat. Rev. Mol. Cell Biol. 8 (2007) 813–824, https://doi.org/10.1038/nrm2256.
[6] L. Wang, J. Tang, L. Wang, et al., Oxidative stress in oocyte aging and female reproduction, J. Cell. Physiol. 236 (2021) 7966–7983, https://doi.org/10.1002/jcp.30468.
[7] M. Kumar, D. Pathak, S. Venkatesh, et al., Chromosomal abnormalities & oxidative stress in women with premature ovarian failure (POF), Indian J. Med. Res. 135 (2012) 92–97, https://doi.org/10.4103/0971-5916.93430.
[8] A. Agarwal, A. Aponte-Mellado, B.J. Premkumar, A. Shaman, S. Gupta, The effects of oxidative stress on female reproduction: a review, Reprod. Biol. Endocrinol. : RBE (Rev. Bras. Entomol.) 10 (2012) 49, https://doi.org/10.1186/1477-7827-10-49.
[9] D.L. Russell, R.L. Robker, Molecular mechanisms of ovulation: co-ordination through the cumulus complex, Hum. Reprod. Update 13 (2007) 289–312, https://doi.org/10.1093/humupd/dml062.
[10] E.A. McGee, A.J. Hsueh, Initial and cyclic recruitment of ovarian follicles, Endocr. Rev. 21 (2000) 200–214, https://doi.org/10.1210/edrv.21.2.0394.
[11] A.J. Hsueh, K. Kawamura, Y. Cheng, B.C. Fauser, Intraovarian control of early folliculogenesis, Endocr. Rev. 36 (2015) 1–24, https://doi.org/10.1210/er.2014-1020.
[12] X.Y. Zhou, J. Zhang, Y. Li, et al., Advanced oxidation protein products induce G1/G0-phase Arrest in ovarian granulosa cells via the ROS-JNK/p38 MAPK-p21 pathway in premature ovarian insufficiency, Oxid. Med. Cell. Longev. 2021 (2021), 6634718, https://doi.org/10.1155/2021/6634718.
[13] X. Lin, Y. Dai, X. Tong, et al., Excessive oxidative stress in cumulus granulosa cells induced cell senescence contributes to endometriosis-associated infertility, Redox Biol. 30 (2020), 101431, https://doi.org/10.1016/j.redox.2020.101431.
[14] M. Appasamy, E. Jauniaux, P. Serhal, et al., Evaluation of the relationship between follicular fluid oxidative stress, ovarian hormones, and response to gonadotropin stimulation, Fertil. Steril. 89 (2008) 912–921, https://doi.org/10.1016/j.fertnstert.2007.04.034.
[15] N. Zhang, Y. Shen, H. Li, et al., The m6A reader IGF2BP3 promotes acute myeloid leukemia progression by enhancing RCC2 stability, Exp. Mol. Med. 54 (2022) 194–205, https://doi.org/10.1038/s12276-022-00735-x.
[16] J.N. Wang, F. Wang, J. Ke, et al., Inhibition of METTL3 attenuates renal injury and inflammation by alleviating TAB3 m6A modifications via IGF2BP2-dependent mechanisms, Sci. Transl. Med. 14 (2022), eabk2709, https://doi.org/10.1126/scitranslmed.abk2709.
[17] P. Zhu, F. He, Y. Hou, et al., A novel hypoxic long noncoding RNA KB-1980E6.3 maintains breast cancer stem cell stemness via interacting with IGF2BP1 to facilitate c-Myc mRNA stability, Oncogene 40 (2021) 1609–1627, https://doi.org/10.1038/s41388-020-01638-9.
[18] T. Xue, X. Liu, M. Zhang, et al., PADI2-Catalyzed MEK1 citrullination activates ERK1/2 and promotes IGF2BP1-mediated SOX2 mRNA stability in endometrial cancer, Adv. Sci. 8 (2021), 2002831, https://doi.org/10.1002/advs.202002831.
[19] I.A. Elcheva, T. Wood, K. Chiarolanzio, et al., RNA-binding protein IGF2BP1 maintains leukemia stem cell properties by regulating HOXB4, MYB, and ALDH1A1, Leukemia 34 (2020) 1354–1363, https://doi.org/10.1038/s41375-019-0656-9.
[20] S. Müller, N. Bley, B. Busch, et al., The oncofetal RNA-binding protein IGF2BP1 is a druggable, post-transcriptional super-enhancer of E2F-driven gene expression in cancer, Nucleic Acids Res. 48 (2020) 8576–8590, https://doi.org/10.1093/nar/gkaa653.
[21] A.E. Conway, E.L. Van Nostrand, G.A. Pratt, et al., Enhanced CLIP uncovers IMP protein-RNA targets in human pluripotent stem cells important for cell adhesion and survival, Cell Rep. 15 (2016) 666–679, https://doi.org/10.1016/j.celrep.2016.03.052.
[22] Y. Wang, J. Zhang, Y. Su, et al., miRNA-98-5p targeting IGF2BP1 induces mesenchymal stem cell apoptosis by modulating PI3K/akt and p53 in immune thrombocytopenia, Mol. Ther. Nucleic Acids 20 (2020) 764–776, https://doi.org/10.1016/j.omtn.2020.04.013.
[23] P. Chatterji, P.A. Williams, K.A. Whelan, et al., Posttranscriptional regulation of colonic epithelial repair by RNA binding protein IMP1/IGF2BP1, EMBO Rep. 20 (2019), https://doi.org/10.15252/embr.201847074.
[24] V. Singh, C.P. Gowda, V. Singh, et al., The mRNA-binding protein IGF2BP1 maintains intestinal barrier function by up-regulating occludin expression, J. Biol. Chem. 295 (2020) 8602–8612, https://doi.org/10.1074/jbc.AC120.013646.
[25] A. Tiwari, K. Tashiro, A. Dixit, et al., Loss of HIF1A from pancreatic cancer cells increases expression of PPP1R1B and degradation of p53 to promote invasion and metastasis, Gastroenterology 159 (2020) 1882–1897, https://doi.org/10.1053/j.gastro.2020.07.046, e1885.
[26] H. Li, H. Zhang, G. Huang, et al., Loss of RPS27a expression regulates the cell cycle, apoptosis, and proliferation via the RPL11-MDM2-p53 pathway in lung adenocarcinoma cells, J. Exp. Clin. Cancer Res. : CR (Clim. Res.) 41 (2022) 33, https://doi.org/10.1186/s13046-021-02230-z.
[27] S. Shangary, S. Wang, Targeting the MDM2-p53 interaction for cancer therapy, Clin. Cancer Res. 14 (2008) 5318–5324, https://doi.org/10.1158/1078-0432.Ccr-07-5136.
[28] A.M. Klein, R.M. de Queiroz, D. Venkatesh, C. Prives, The roles and regulation of MDM2 and MDMX: it is not just about p53, Gene Dev. 35 (2021) 575–601, https://doi.org/10.1101/gad.347872.120.
[29] G. Arena, M.Y. Cissé, S. Pyrdziak, et al., Mitochondrial MDM2 regulates respiratory complex I activity independently of p53, Mol. Cell. 69 (2018) 594–609, https://doi.org/10.1016/j.molcel.2018.01.023, e598.
[30] Y. Li, Y. Xiang, Y. Song, D. Zhang, L. Tan, MALAT1 downregulation is associated with polycystic ovary syndrome via binding with MDM2 and repressing P53 degradation, Mol. Cell. Endocrinol. 543 (2022), 111528, https://doi.org/10.1016/j.mce.2021.111528.
[31] H. Haraguchi, Y. Hirota, T. Saito-Fujita, et al., Mdm2-p53-SF1 pathway in ovarian granulosa cells directs ovulation and fertilization by conditioning oocyte quality, Faseb. J. : official publication of the Federation of American Societies for Experimental Biology 33 (2019) 2610–2620, https://doi.org/10.1096/fj.201801401R.
[32] J.H. Park, S.A. Park, Y.J. Lee, et al., TOPK inhibition accelerates oxidative stress-induced granulosa cell apoptosis via the p53/SIRT1 axis, Int. J. Mol. Med. 46 (2020) 1923–1937, https://doi.org/10.3892/ijmm.2020.4712.
[33] A. Gal, P.C. Lin, A.M. Barger, A.L. MacNeill, C. Ko, Vaginal fold histology reduces the variability introduced by vaginal exfoliative cytology in the classification of mouse estrous cycle stages, Toxicol. Pathol. 42 (2014) 1212–1220, https://doi.org/10.1177/0192623314526321.
[34] K.L. Gabrielson, B.A. Hogue, V.A. Bohr, et al., Mitochondrial toxin 3-nitropropionic acid induces cardiac and neurotoxicity differentially in mice, Am. J. Pathol. 159 (2001) 1507–1520, https://doi.org/10.1016/s0002-9440(10)62536-9.

[35] J.B. Schulz, D.R. Henshaw, U. MacGarvey, M.F. Beal, Involvement of oxidative stress in 3-nitropropionic acid neurotoxicity, Neurochem. Int. 29 (1996) 167–171, https://doi.org/10.1016/0197-0186(95)00122-0.
[36] C.C. Hsieh, J. Papaconstantinou, The effect of aging on p38 signaling pathway activity in the mouse liver and in response to ROS generated by 3-nitropropionic acid, Mech. Ageing Dev. 123 (2002) 1423–1435, https://doi.org/10.1016/s0047-6374(02)00084-2.
[37] J.C. Patterson, B.A. Joughin, B. van de Kooij, et al., ROS and oxidative stress are elevated in mitosis during asynchronous cell cycle progression and are exacerbated by mitotic arrest, Cell Syst 8 (2019) 163–167, https://doi.org/10.1016/j.cels.2019.01.005, e162.
[38] E. Ghosh, A. Ghosh, A.N. Ghosh, T. Nozaki, S. Ganguly, Oxidative stress-induced cell cycle blockage and a protease-independent programmed cell death in microaerophilic Giardia lamblia, Drug Des. Dev. Ther. 3 (2009) 103–110, https://doi.org/10.2147/dddt.s5270.
[39] J.G. Pizarro, J. Folch, A. Vazquez De la Torre, et al., Oxidative stress-induced DNA damage and cell cycle regulation in B65 dopaminergic cell line, Free Radic. Res. 43 (2009) 985–994, https://doi.org/10.1080/10715760903159188.
[40] I. Liguori, G. Russo, F. Curcio, et al., Oxidative stress, aging, and diseases, Clin. Interv. Aging 13 (2018) 757–772, https://doi.org/10.2147/cia.S158513.
[41] Z. Yang, T. Wang, D. Wu, et al., RNA N6-methyladenosine reader IGF2BP3 regulates cell cycle and angiogenesis in colon cancer, J. Exp. Clin. Cancer Res. : CR (Clim. Res.) 39 (2020) 203, https://doi.org/10.1186/s13046-020-01714-8.
[42] J. Cui, J. Tian, W. Wang, et al., IGF2BP2 promotes the progression of colorectal cancer through a YAP-dependent mechanism, Cancer Sci. 112 (2021) 4087–4099, https://doi.org/10.1111/cas.15083.
[43] F. Sperling, D. Misiak, S. Hüttelmaier, P. Michl, H. Griesmann, IGF2BP1 promotes proliferation of neuroendocrine neoplasms by post-transcriptional enhancement of EZH2, Cancers 14 (2022), https://doi.org/10.3390/cancers14092121.
[44] V. Gorgoulis, P.D. Adams, A. Alimonti, et al., Cellular senescence: defining a path forward, Cell 179 (2019) 813–827, https://doi.org/10.1016/j.cell.2019.10.005.
[45] F. Xie, C. Huang, F. Liu, et al., CircPTPRA blocks the recognition of RNA N(6)-methyladenosine through interacting with IGF2BP1 to suppress bladder cancer progression, Mol. Cancer 20 (2021) 68, https://doi.org/10.1186/s12943-021-01359-x.
[46] Y. Zhou, P. Zeng, Y.H. Li, Z. Zhang, Q. Cui, SRAMP: prediction of mammalian N6-methyladenosine (m6A) sites based on sequence-derived features, Nucleic Acids Res. 44 (2016) e91, https://doi.org/10.1093/nar/gkw104.
[47] H.Y. Fan, Z. Liu, M. Shimada, et al., MAPK3/1 (ERK1/2) in ovarian granulosa cells are essential for female fertility, Science (New York, N.Y.) 324 (2009) 938–941, https://doi.org/10.1126/science.1171396.
[48] H.M. Chang, J. Qiao, P.C. Leung, Oocyte-somatic cell interactions in the human ovary-novel role of bone morphogenetic proteins and growth differentiation factors, Hum. Reprod. Update 23 (2016) 1–18, https://doi.org/10.1093/humupd/dmw039.
[49] S.J. Chon, Z. Umair, M.S. Yoon, Premature ovarian insufficiency: past, present, and future, Front. Cell Dev. Biol. 9 (2021), 672890, https://doi.org/10.3389/fcell.2021.672890.
[50] M. Das, O. Djahanbakhch, B. Hacihanefioglu, et al., Granulosa cell survival and proliferation are altered in polycystic ovary syndrome, J. Clin. Endocrinol. Metab. 93 (2008) 881–887, https://doi.org/10.1210/jc.2007-1650.
[51] A.M. Sanchez, E. Somigliana, P. Vercellini, et al., Endometriosis as a detrimental condition for granulosa cell steroidogenesis and development: from molecular alterations to clinical impact, J. Steroid Biochem. Mol. Biol. 155 (2016) 35–46, https://doi.org/10.1016/j.jsbmb.2015.07.023.
[52] J.A. Klein, S.L. Ackerman, Oxidative stress, cell cycle, and neurodegeneration, J. Clin. Invest. 111 (2003) 785–793, https://doi.org/10.1172/jci18182.
[53] J.M. Matés, J.A. Segura, F.J. Alonso, J. Márquez, Intracellular redox status and oxidative stress: implications for cell proliferation, apoptosis, and carcinogenesis, Arch. Toxicol. 82 (2008) 273–299, https://doi.org/10.1007/s00204-008-0304-z.
[54] J. Cui, Y. Li, W. Zhang, et al., Alginic acid induces oxidative stress-mediated hormone secretion disorder, apoptosis and autophagy in mouse granulosa cells and ovaries, Toxicology 467 (2022), 153099, https://doi.org/10.1016/j.tox.2022.153099.
[55] J.Q. Zhang, B.W. Gao, J. Wang, et al., Critical role of FoxO1 in granulosa cell apoptosis caused by oxidative stress and protective effects of grape seed procyanidin B2, Oxid. Med. Cell. Longev. 2016 (2016), 6147345, https://doi.org/10.1155/2016/6147345.
[56] H. Huang, H. Weng, W. Sun, et al., Recognition of RNA N(6)-methyladenosine by IGF2BP proteins enhances mRNA stability and translation, Nat. Cell Biol. 20 (2018) 285–295, https://doi.org/10.1038/s41556-018-0045-z.
[57] T. Gutschner, M. Hämmerle, N. Pazaitis, et al., Insulin-like growth factor 2 mRNA-binding protein 1 (IGF2BP1) is an important protumorigenic factor in hepatocellular carcinoma, Hepatology 59 (2014) 1900–1911, https://doi.org/10.1002/hep.26997.
[58] N.A. Manieri, M.R. Drylewicz, H. Miyoshi, T.S. Stappenbeck, Igf2bp1 is required for full induction of Ptgs2 mRNA in colonic mesenchymal stem cells in mice, Gastroenterology 143 (2012) 110–121, https://doi.org/10.1053/j.gastro.2012.03.037, e110.
[59] S. Ke, E.A. Alemu, C. Mertens, et al., A majority of m6A residues are in the last exons, allowing the potential for 3' UTR regulation, Gene Dev. 29 (2015) 2037–2053, https://doi.org/10.1101/gad.269415.115.
[60] K.D. Meyer, Y. Saletore, P. Zumbo, et al., Comprehensive analysis of mRNA methylation reveals enrichment in 3' UTRs and near stop codons, Cell 149 (2012) 1635–1646, https://doi.org/10.1016/j.cell.2012.05.003.
[61] P. Chène, Inhibiting the p53–MDM2 interaction: an important target for cancer therapy, Nat. Rev. Cancer 3 (2003) 102–109, https://doi.org/10.1038/nrc991.
[62] Z. Wang, H. Dong, L. Yang, et al., The role of FDX1 in granulosa cell of Polycystic ovary syndrome (PCOS), BMC Endocr. Disord. 21 (2021) 119, https://doi.org/10.1186/s12902-021-00775-w.